sustainability

MDPI

Article

Effects of Surge Tank Geometry on the Water Hammer Phenomenon: Numerical Investigation

Mohammad Mahmoudi-Rad [1,*] and Mohammad Najafzadeh [2]

[1] Department of Civil Engineering, Higher Education Complex of Bam, Bam P.O. Box 76615314, Iran
[2] Department of Water Engineering, Faculty of Civil and Surveying Engineering, Graduate University of Advanced Technology, Kerman P.O. Box 76315116, Iran
* Correspondence: m.m6456@yahoo.com or m.mahmoudirad@bam.ac.ir

Abstract: A surge tank, as one of the most common control facilities, is applied to control head pressure levels in long pressurized pipelines during the water hammer occurrence. The cost-effective operation of surge tanks is highly affected by their characteristics (i.e., surge tank diameter and inlet diameter of surge tanks) and can effectively reduce the repercussion of water hammers. This investigation utilized the method of characteristics (MOC) in order to simulate the behavior of transient flow at the surge tank upstream and the head pressure fluctuations regime for the hydraulic system of a hydropower dam. Firstly, the MOC model was validated by experimental observations. The various types of boundary conditions (i.e., sure tank, reservoir, branch connection of three pipes, series pipes, and downstream valve) were applied to investigate the simultaneous effects of the surge tank properties. In this way, all the simulations of water hammer equations were conducted for nine various combinations of surge tank diameter (D) and inlet diameter of surge tank (d). The results of this study indicated that for the surge tank design with D = 6 m and d = 3.4 m, head pressure fluctuations reached the minimum level in the large section of the pipeline which is the surge tank upstream. Additionally, the occurrence of the water hammer phenomenon was probable in the initial section of the pipeline.

Keywords: water hammer; transient flow fluctuations; method of characteristics; surge tank

Citation: Mahmoudi-Rad, M.; Najafzadeh, M. Effects of Surge Tank Geometry on the Water Hammer Phenomenon: Numerical Investigation. *Sustainability* **2023**, *15*, 2312. https://doi.org/10.3390/su15032312

Academic Editor: Miklas Scholz

Received: 24 November 2022
Revised: 20 January 2023
Accepted: 24 January 2023
Published: 27 January 2023

1. Introduction

Water hammer occurrence is one of the most destructive hydraulic phenomena in water distribution systems. This issue takes place in the event that flow velocity and pressure values vary suddenly in some cases such as sudden opening and closing valves, accidents of the pump, and unexpectedly depressurized hydraulic systems. Overall, water hammer takes place in various hydraulic systems such as pump stations [1–4], hydro-power systems [5–7], water-transferring systems [8–12], and oil-transferring systems [13,14].

Water hammer causes damages in different ways (*i*) severe fluctuations in pressure and noise, (*ii*) cavitation occurrence in the hydraulic systems. Specifically, instant positive and negative pressure occurred during the water hammer phenomenon stands at a higher level than operation pressure. Positive pressure causes damage to the valves and pipe burst whereas negative pressure crushes the pipe systems.

Applying preventative methods to eradicate the repercussions of the water hammer phenomena has become the cornerstone of experts in the hydraulic fields. Through this issue, the maximum reduction of maximum pressure values and a maximum increase of minimum pressure values have drawn significant attention to the control of water hammer occurrences in recent decades. In this way, these methods generally include the installation of control facilities of water hammer and optimization of facilities performance [15,16]. Improvement of policy for the closing valve and coordinated performance of the hydraulic systems is one of the most common optimization methods to control the water hammer phenomenon [17–19].

Moreover, optimizing the performance of the hydraulic systems is not essentially capable of controlling the water hammer and there is an occasional need for protective pieces of a device for this aim. Generally, surge tanks, relief valves, and pressure tanks are the most well-known pieces of equipment to control the water hammer [16]. However, surge tanks are one of the most widely used protection devices to reduce the water hammer. These tanks are very popular in water transmission systems, pumping systems, and power plant systems. Although a large number of attempts were made on surge tanks, they are still being developed to investigate responses of the surge tank to the variations of surge tank geometry. It should be noted that severe fluctuations in water level may cause frequent emptying and filling of the tank in the water hammer occurrence. Therefore, having a sufficient cross section and vertical height is essential. As a result, the lack of space and necessary height occasionally limit the coordinated operation of surge tanks. However, in the case of the above-mentioned problems, surge tanks are not well capable of controlling the severe fluctuations caused by the water hammer.

Laboratory and numerical investigations have been conducted to simulate transient hydraulic flows occurring in the water hammer. However, in the case of laboratory simulations, it is very difficult to combine various boundary conditions. In addition, performing an experimental study is highly time-consuming time and expensive. With the development of computers and computational methodologies, numerical techniques are being used more widely to simulate the water hammer in various engineering applications. In this case, numerical methods are grouped into three main categories: the Finite Difference Method (FDM), Finite Element Method (FEM), and Finite Volume Method (FVM). Over the past few decades, various numerical methods have been developed to simulate and control transient hydraulic flows during the water hammer phenomenon. The most commonly used FDMs is the Method of Characteristics (MOC) with explicit form, which has been widely applied and improved in multi-pipe hydraulic systems [15,20–23]. In the case of MOC applications, the recent investigations have been in relation to (*i*) improvement of MOC by Non-Dominated Sorting Genetic Algorithm II (NSGA II) for finding the response of chamber surge tank of water hammer [24], (*ii*) MOC application for water hammer simulation in offshore floating production unit [25], (*iii*) control of water hammer for additional High-Density Polyethylene (HDPE) pipeline systems by MOC simulation [26], and (*iv*) MOC simulation of water hammer phenomenon for pressurized pipelines [27].

In recent years, the effects of the inlet cross-section and the length of the inlet junction associated with the surge tank on the response of the surge tank have been investigated [16,23]. According to the literature [15,20–27], simultaneous influences of surge tank properties (i.e., surge tank diameter and inlet diameter of surge tank) have not yet been studied. The simultaneous use of surge tank properties causes finding an efficient design of water systems and therefore this case requires more consideration in the design of water systems. Hence, in this study, the performance of the surge tank, installed on the pipeline of the Jiroft Dam powerhouse, is studied to reduce the repercussion of the water hammer phenomenon. On the other hand, the optimal combinations of these factors that are effective in the proper control of transient flow fluctuations are introduced. In this way, the MOC, introduced as the most well-known FDMs in this research area, is used to simulate the response of the water system along with various boundary conditions in the pipeline such as triple-shaped junctions, series pipelines, and control valves downstream of the power plant model. Ultimately, the effects of various elements would be evaluated.

1.1. Overview of Power Plant Model

The power plant case study was constructed for the Jiroft Hydroelectric Dam, located in the southeast of Iran. The reservoir capacity contains approximately 410 million cubic meters up to 1185 m above sea level. Figure 1 shows the details of the hydraulic system of the power plant, including the upstream reservoir, the branch connection of triple pipes, the surge tank, the connection of two series pipes, and the valve downstream.

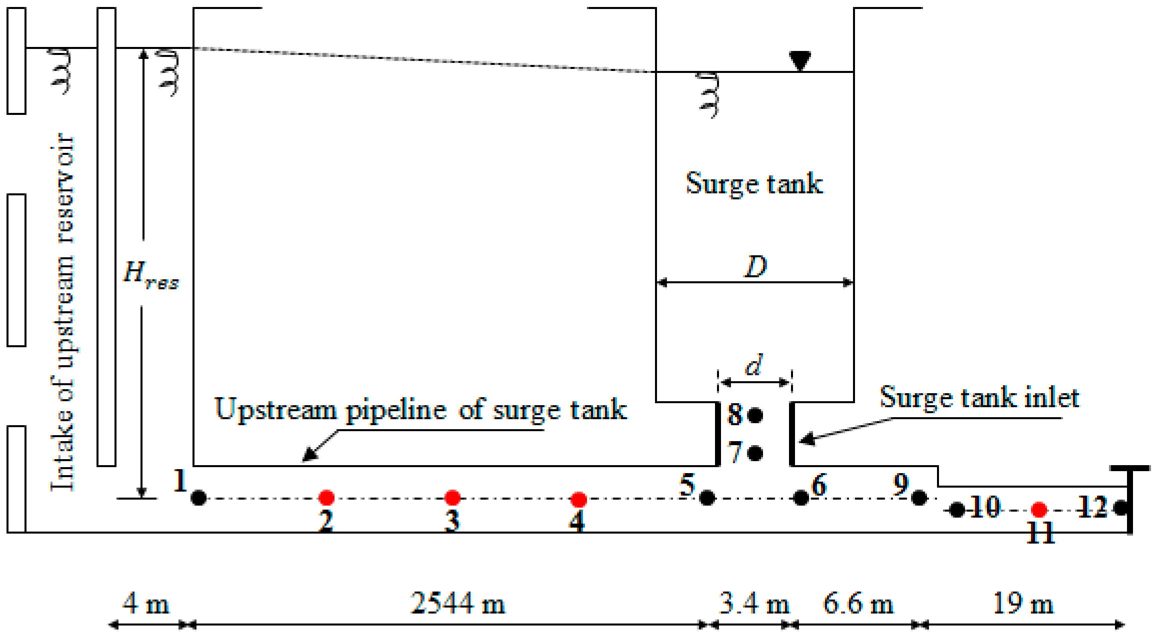

Figure 1. Schematic diagram of the main sections of the power plant: red points describe points of grid without boundary conditions; black points express boundary conditions of the MOC scheme.

The upstream pipe of the surge tank with a length of 2544 m and a diameter of 3.4 m is connected to a three-way junction with the same diameter. The inlet diameter of the surge tank (d) and the diameter of the surge tank (D) are 3.4 m and 6 m, respectively. The system response to the variations in D and d variables is assessed by ±20% variations in these factors. There is only one assumption in this paper. ±20% variations of two geometric parameters (d and D) caused to quantify transient flow characteristics variations. The rest of the parameters such as boundary conditions (i.e., series connections, surge tank, upstream reservoir, branch connection of three pipes, downstream valve) are taken into consideration according to the availability of water pipeline elements. Additionally, two parameters of time and space intervals were assigned to obtain courant numbers below one, and they are in relation to the conditions of the MOC solution scheme. Regarding the reason for choosing higher (1.2d and 1.2D) and lower (0.8d and 0.8D) levels for each of the geometric parameters, it should be said that this type of selection led to the best indication of the trend of the results versus smaller and larger values of the parameters. Therefore, this will help to choose the optimal combination of these factors in order to reach a more confident conclusion. Values greater than 20%, in addition to greatly increasing the implementation costs, cause unprincipled and inappropriate combinations between the two factors of the inlet diameter of the surge tank and the diameter of the surge tank. As an assumption, we can point out a 40% increase in the diameter of the inlet to the surge tank and the combination of this value with a 40% decrease in the diameter of the surge tank, which is not practical or suitable at all. With this assumption, the diameter of the inlet to the surge tank is 4.76 m and the diameter of the surge tank is 3.6 m, which is smaller than the diameter of the inlet to the surge tank, and these values are not consistent with the design of the surge tanks. There are two series pipes with diameters of 2.4 m and 3.4 m which are placed downstream of the power plant model. The friction factor of the system pipes is 0.016. In order to investigate and analyze the water hammer phenomenon in different parts of the system, 12 nodes have been located. Nodes 1 to 5 on the upstream pipe, 5 to 7 for the three-way connection, node 8 for the surge tank, nodes 9 and 10 for the series connection of the two pipes, node 11 for the end pipe, and node 12 for the control valve at the end of the line path. Pipes are considered. In the initial conditions, the level of the head pressure in nodes 1, 8, and 12 are 67 m, 62.28 m, and 62.06 m, respectively.

1.2. Equations Governing Transient Flows

The set of physical equations corresponding to fluid motion includes the continuity equation, the motion size equation, and the energy equation. For one-dimensional flow in a closed-ended pipe (as an isothermal process without energy conversion), the governing equations of flow are the equations of continuity and momentum. Therefore, the following equations can be considered for the transient flow regime in the pipe [28]:

$$\begin{cases} L_1 = h_t + \frac{a^2}{g} v_x + v h_x + v \sin\theta = 0 \\ L_2 = v_t + g h_x + v v_x + f \frac{v|v|}{2D_P} = 0 \end{cases} \tag{1}$$

where h is the head pressure, v is the flow velocity, a is the wave speed of the water hammer, g is the gravity acceleration, θ is the pipe slope, D_p is the pipeline diameter, t subscript is the derivative of a variable respect to time, and x is derivative of a variable respect to space.

1.3. Overview of MOC

The Method Of Characteristics (MOC) has been widely applied to simulate the transient flow for various situations: water pipeline [11,12], power plant [5,6], and water pump station [2,3].

For this purpose, Equation (1) is converted to the linear combination of $L1$ and $L2$ as $L1 + \lambda L2 = 0$, in which $\lambda = \pm g/a$ and $dx/dt = v \pm a$. In this way, Equation (1) is re-expressed as

$$\begin{cases} C^+ : \frac{g}{a} h_t + v_t + \frac{g}{a} v \sin\theta + f \frac{v|v|}{2D_P} = 0\,,\ dx/dt = v + a \\ C^- : -\frac{g}{a} h_t + v_t - \frac{g}{a} v \sin\theta + f \frac{v|v|}{2D_P} = 0\,,\ dx/dt = v - a \end{cases} \tag{2}$$

The schematic diagram of MOC was conceptually illustrated in Figure 2. As seen in Figure 2, flow velocity and head pressure values which are associated with nodes 2, 3, 4, and 11 (see Figure 1), are obtained as

$$\begin{cases} C^+ : (v_P - v_L) + \frac{g}{a}(h_P - h_L) + \frac{g}{a} v_L \sin\theta (t_P - t_L) + f \frac{v_L|v_L|}{2D_P} (t_P - t_L) = 0 \\ \qquad (x_P - x_L) = (v_L + a)(t_P - t_L) \\ C^- : (v_P - v_R) - \frac{g}{a}(h_P - h_R) - \frac{g}{a} v_R \sin\theta (t_P - t_R) + f \frac{v_R|v_R|}{2D_P} (t_P - t_R) = 0 \\ \qquad (x_P - x_R) = (v_R - a)(t_P - t_R) \end{cases} \tag{3}$$

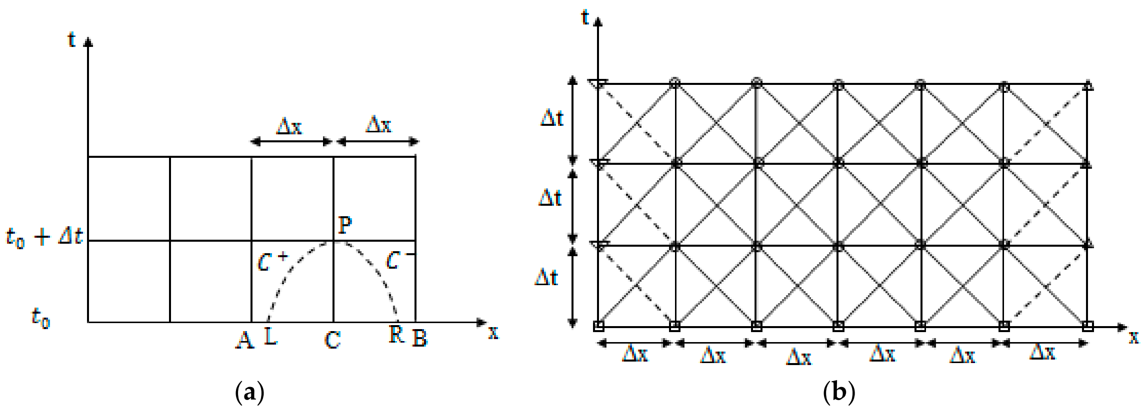

Figure 2. Schematic illustration of MOC: (**a**) Characteristic lines in the x-t plane and (b) general grid points of MOC.

In the above-mentioned equation, v_L, v_R, h_L, and h_R are initially computed by interpolation as,

$$\begin{cases} v_L = v_C - a(v_C - v_A)\Delta t/\Delta x \\ v_R = v_C - a(v_C - v_B)\Delta t/\Delta x \\ h_L = h_C - a(h_C - h_A)\Delta t/\Delta x \\ h_R = h_C - a(h_C - h_B)\Delta t/\Delta x \end{cases} \tag{4}$$

Equation (4) is substituted into Equation (1) and then h_P and v_P are computed as,

$$\begin{cases} v_P = 0.5\left[v_L + v_R + \frac{g}{a}(h_L - h_R) - \frac{g}{a}\Delta t \sin\theta(v_L - v_R) - \frac{f\Delta t}{2D_P}(v_L|v_L| + v_R|v_R|)\right] \\ h_P = 0.5\left[h_L + h_R + \frac{a}{g}(v_L - v_R) - \Delta t \sin\theta(v_L + v_R) - \frac{a}{g}\frac{f\Delta t}{2D_P}(v_L|v_L| - v_R|v_R|)\right] \end{cases} \tag{5}$$

To compute h_P and v_P for other nodes, boundary conditions need to be investigated.

In this study, the wave speed of transient flow (a) for the pipeline at the surge tank upstream (d = 3.4 m) is 1150 m/s whereas, for the pipeline at the surge tank downstream (d = 2.4 m), is 1300 m/s. To implement MOC for the simulation of head pressure and flow velocity variations in the present hydraulic systems, Δt and Δx are fixed as 0.3 s and 390 m, respectively. Furthermore, the MOC programming code was provided in MATLAB.

1.4. Boundary Conditions

Compared to the literature [20–27], this study would apply five boundary conditions (i.e., series connections, surge tank, upstream reservoir, branch connection of three pipes, downstream valve) to evaluate pressure heads along water pipelines. In this way, the scheme of the MOC solution would be more complicated than that of previous studies. Applying the complexity of boundary conditions depends on the availability of elements of water distribution systems such as valves, variation of pipeline cross-section, junction, reservoir, and pump.

1.5. Upstream Reservoir

Figure 3 illustrates the boundary condition of the reservoir upstream. According to this, equation governed by the reservoir upstream is expressed as [28],

$$\begin{cases} & h_{p_{j,1}} = H_{res} \\ C^- : & v_{p_{j,1}} = C1_j + C2_j\, h_{p_{j,1}} \\ & C1 = v_R - C2\, h_R + C2\, v_R \sin\theta\, \Delta t - \frac{f\Delta t}{2D_P}\, v_R\, |v_R|\,,\ C2 = \frac{a}{g} \end{cases} \tag{6}$$

in which j is the number of the pipe and H_{res} is the head pressure of the reservoir upstream.

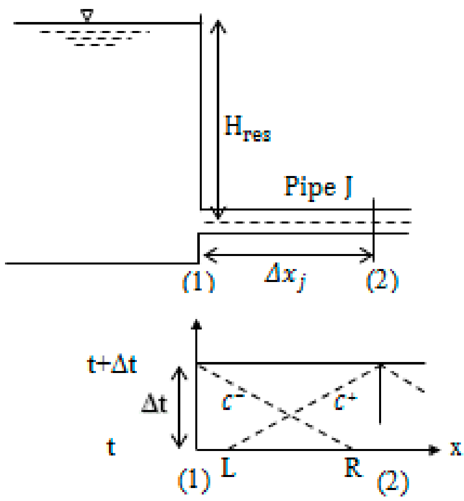

Figure 3. Schematic diagram of boundary condition of reservoir upstream.

1.6. Branch Connection of Three Pipes

According to Figure 1, h_P and v_P are associated with nodes 5, 6, and 7. In fact, the boundary condition of the branch connection of three pipes was studied by these nodes (5–7). Figure 4 depicted this typical boundary condition for nodes 5 to 7 and then the following formulation is expressed to find the flow characteristics for these nodes (5 to 7) as [28],

$$\begin{cases} h_{P_{j,n+1}} = \frac{C3_j A_j - C1_{j+1} A_{j+1} - C1_{j+2} A_{j+2}}{C2_j A_j + C2_{j+1} A_{j+1} + C2_{j+2} A_{j+2}} \\ h_{P_{j+1,1}} = h_{P_{j+2,1}} = h_{P_{j,n+1}} \\ v_{p_{j,n+1}} = C3_j - C2_j \, h_{p_{j,n+1}} \\ v_{p_{j+1,1}} = C1_{j+1} + C2_{j+1} \, h_{p_{j+1,1}} \\ v_{p_{j+2,1}} = C1_{j+2} + C2_{j+2} \, h_{p_{j+2,1}} \\ C3 = v_L + C2 \, h_L - C2 \, v_L \sin\theta \, \Delta t - \frac{f \Delta t}{2 D_P} \, v_L \, |v_L| \end{cases} \quad (7)$$

where the subscript of n denotes the number of the node.

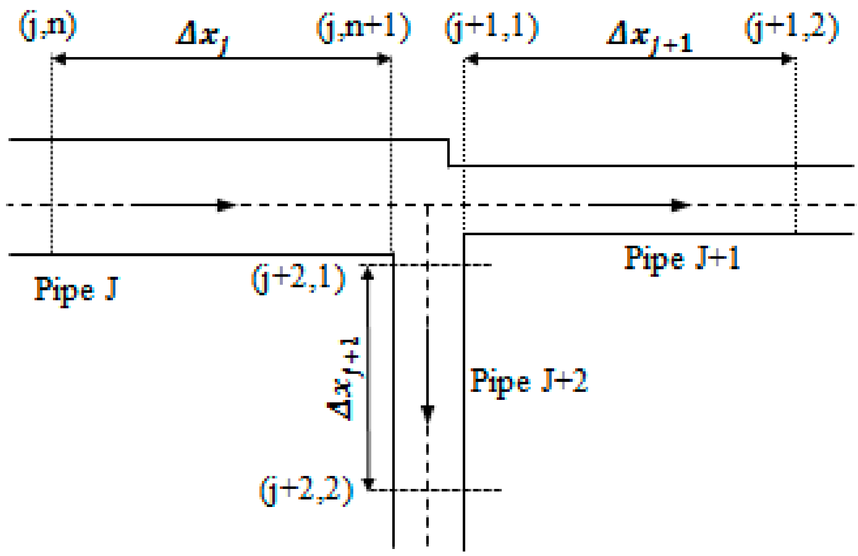

Figure 4. Illustration of boundary condition for branch connection of three pipes.

1.7. Surge Tank

According to Figure 5, h_P and v_P values for node 5 are computed as [28],

$$\begin{cases} h_{p_{j+2,n+1}} = L_{j+2} + ZP \\ ZP = z + v_{p_{j+2,n+1}} A_{j+2} \Delta t / A_s \\ v_{p_{j+2,n+1}} = (C3_{j+2} - C2_{j+2} h_{p_{j+2,n+1}}) / (1 + C2_{j+2} A_{j+2} \Delta t / A_s) \end{cases} \quad (8)$$

where A_s is the cross-section of the surge tank, ZP is the height of the water surface in the surge tank at the end of the time interval, and z denotes is the height of the water surface at the beginning of the time interval.

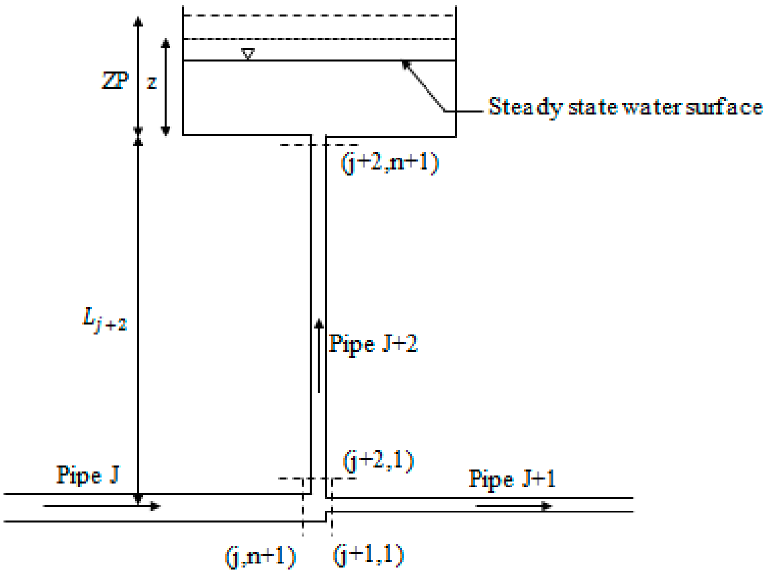

Figure 5. Illustration of boundary condition for the surge tank.

1.8. Series Connection

The schematic diagram of the series connection boundary condition used in this study was illustrated in Figure 6. The boundary conditions for nodes 9 and 10 (as seen in Figure 1) are grouped into typical series connections; therefore, h_P and v_P values are computed as [28],

$$\begin{cases} h_{p_{j,n+1}} = \left(C3_j A_j - C1_{j+1} A_{j+1}\right) / \left(C2_j A_j + C2_{j+1} A_{j+1}\right) \\ h_{p_{j+1,1}} = h_{p_{j,n+1}} \\ C^+ : \; v_{p_{j,n+1}} = C3_j - C2_j h_{p_{j,n+1}} \\ C^- : \; v_{p_{j+1,1}} = C1_{j+1} + C2_{j+1} h_{p_{j+1,1}} \end{cases} \tag{9}$$

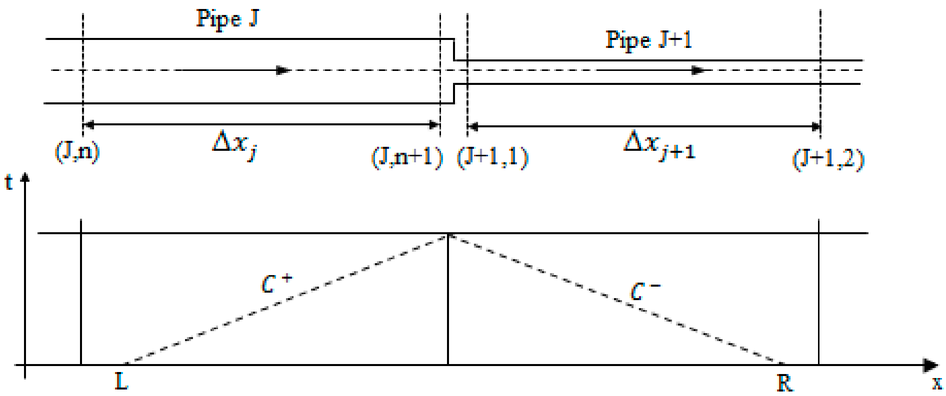

Figure 6. Conceptual depiction of boundary condition for series connection state.

1.9. Downstream Valve

The boundary condition of node 12, as illustrated in Figure 7, includes two states. The first stage is the time when the valve is closed. This situation is expressed by as $\tau = (1 - t/t_c)$ which t_c is the time duration for valve complete closure [28],

$$\begin{cases} c_v = {v_{0_j}}^2 / C2_j H_{0_{j,n+1}} \\ C4 = \tau^2 c_v \\ v_{p_{j,n+1}} = \frac{1}{2} C4 \left(-1 + \sqrt{1 + 4\frac{C3_j}{C4}}\right) \\ h_{p_{j,n+1}} = \left(C3_j - v_{p_{j,n+1}}\right) / C2_j \end{cases} \tag{10}$$

where H_0 is the initial head pressure at the valve.

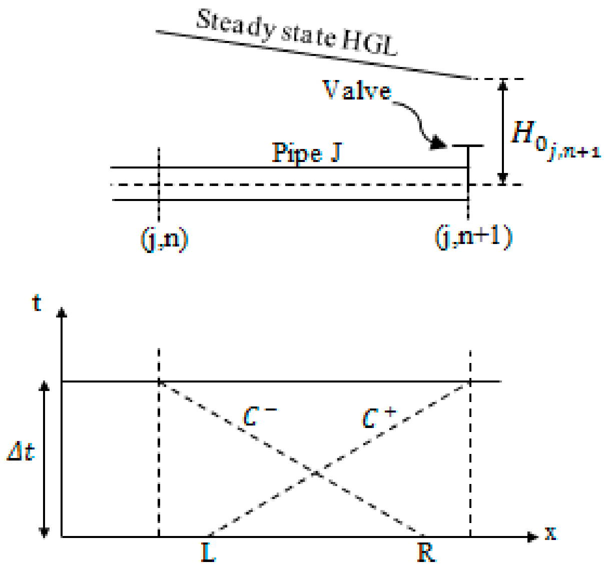

Figure 7. Conceptual depiction of boundary condition for downstream valve state.

The second state of the boundary condition is associated with the time when the valve is completely closed. In this way, the boundary condition for node 12 is expressed as [28],

$$\begin{cases} v_{p_{j,n+1}} = 0 \\ h_{p_{j,n+1}} = C3_j/C2_j \end{cases} \tag{11}$$

1.10. Model Validation

In the case of the proposed model, the results of the numerical validation are compared with the experimental observations conducted by literature Bergant et al. [29]. The proposed numerical scheme is conveniently applied to verify the numerical simulation by the MOC technique. The laboratory facilities include a copper-made pipe with 37.2 m long, 22 mm internal diameter, and wall thickness of 1.63 mm, and a pair of pressurized tanks. In the case of steady-state flow condition, the velocity value, upstream pressurized, valve closure time, wave speed, and the quasi-steady friction coefficient are 0.3 m/s, 32.0 m, 0.09 s, 1319 m/s, and 0.034, respectively. The validation of the MOC scheme needs to investigate the stability limit of the water hammer equations and an acceptable level of stability limit for the solution to the water hammer equations. In this way, the stability limit is identified by the courant condition ($a\Delta t/\Delta x$) which should be less than unity, as fully addressed in the literature review by Pal et al. [30]. This study used the courant condition for the classical MOC solution. In the current research, there are two courant numbers related to the pipelines at the surge tank upstream (C_r = 0.88) and the pipelines at the surge tank downstream (C_r = 1). These courant numbers have been obtained after a large number of trial and error processes between space and time intervals in order to minimize the accuracy level between the results of the MOC scheme and experimental observations. The details of experimental observations can be found in the research of Bergant et al. [29]. Figure 8 illustrates the fluctuation of the transient head pressure values at the endpoint near the valve. As depicted in Figure 8, the classical MOC scheme precisely simulates the maximum values of head pressure.

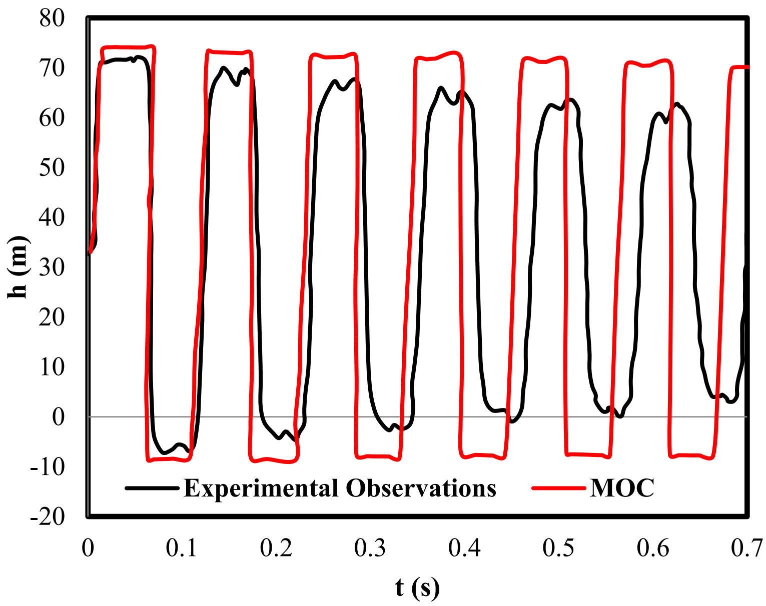

Figure 8. Comparison of the transient head pressure fluctuations by the numerical model at the endpoint with experimental observations.

2. Results and Discussion

2.1. Response of Surge Tank

In this section, the variation of transient flow characteristics (pressure and velocity) associated with the surge tank is investigated. Figure 9a illustrates variations in transient head pressure versus time for the surge tank. As seen in Figure 9a, 9.10 m difference between the peak pressure head (H_{max}) and trough pressure head (H_{min}) was depicted in the initially developed transient flow during the fast-closing valve. The difference between H_{max} and H_{min} decreased to 1.08 m in the middle of the time period. The head pressure of the surge tank remained constant (66.56 m) in the last of the time period. Moreover, variations of transient flow velocity against time (for node 8 in Figure 1) were illustrated in Figure 9b. Maximum fluctuations of transient flow velocity were 13.76 m/s at the beginning of transient flow formation and then this value decreased to 1.37 m/s in the middle time period. Additionally, variations of minimum and maximum head pressure in the surge tank were shown in Figure 10.

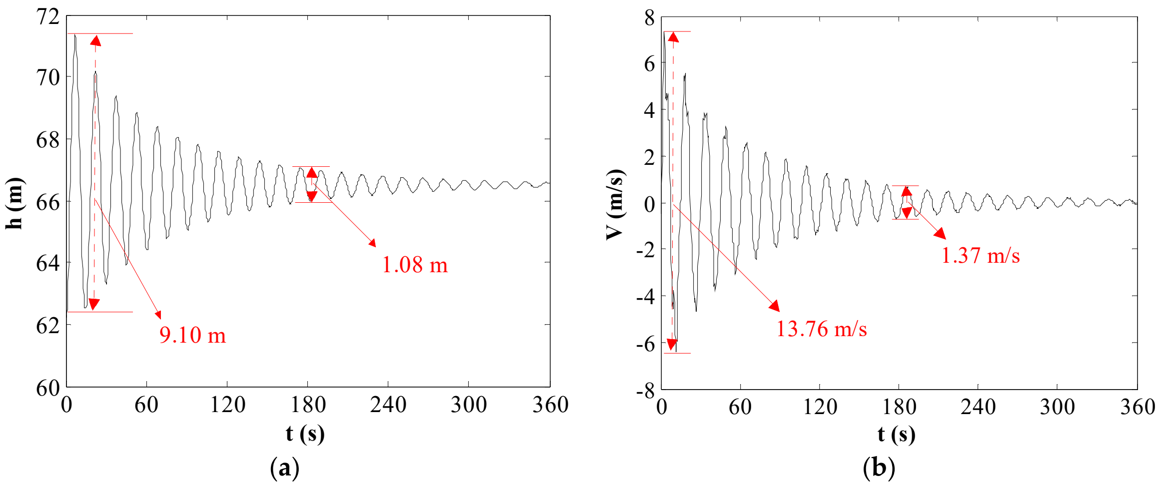

Figure 9. Variations of transient flow properties in the surge tank versus time: (**a**) head pressure and (**b**) flow velocity.

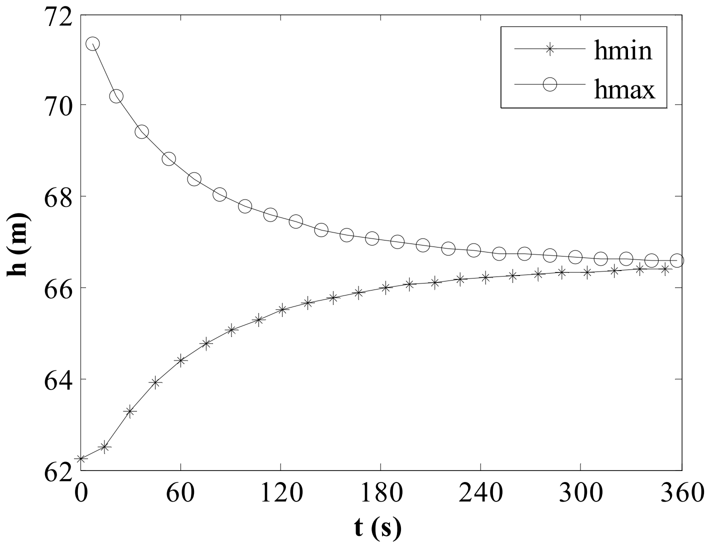

Figure 10. Variations of minimum and maximum peaks associated with head pressure in the surge tank.

2.2. Response of Surge Tank Due to Inlet Diameter Variation

Figure 11 indicates variations of surge tank response versus inlet diameter (d). In this study, variations of d were considered as $d \pm 0.2d$. Figure 11a illustrates variations in head pressure for various surge tank inlet diameters. Maximum variation in the head pressure of the surge tank decreased from 9.10 m to 8.95 m as the d value increased from 3.4 m to 4.08 m. In the case of a 20% decrease in d value, maximum head pressure remained constant at 9.1 m. As illustrated in Figure 11a, with passing time, fluctuations of head pressure for d = 2.72 m stood at the lower level of d = 3.4 m and 4.08 m. Variations of transient flow velocity versus various d values were shown in Figure 11b. Results indicated that the maximum fluctuation of transient flow velocity decreased from 13.76 m/s in d = 3.4 m to 9.23 m/s in d = 4.08 m. In contrast, as the d value decreases from 3.4 m to 2.72 m, the maximum fluctuation of flow velocity in the transient state augments from 13.76 m/s to 20.63 m/s.

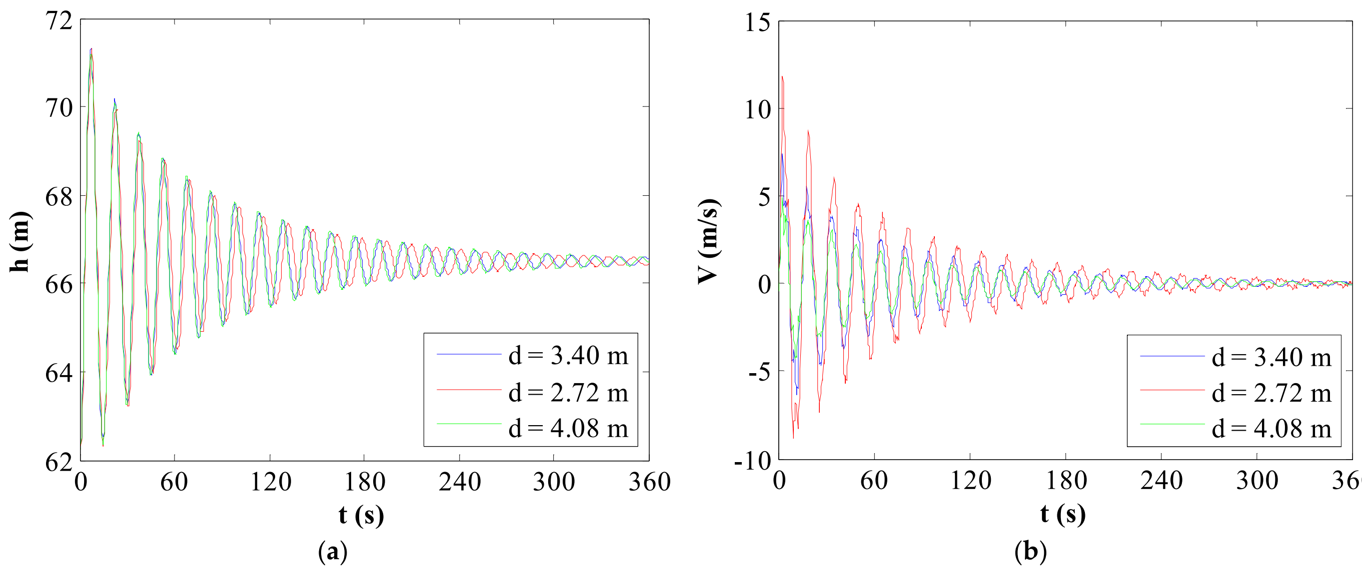

Figure 11. Variations of surge tank response versus inlet diameter: (**a**) head pressure and (**b**) flow velocity.

With reference to Figure 12, the pressure head of the surge tank was on the rise when flow velocity had a positive value. On the contrary, negative values of flow velocity, introduced as flow direction from the surge tank to the pipeline, cause an increase in the head pressure in the surge tank. On the other hand, as the pressure head increased, the surge tank absorbed water from the pipeline to prevent the increase in pressure fluctuation.

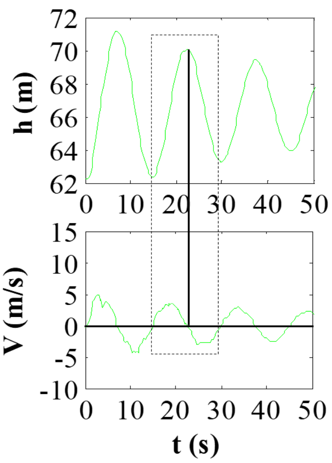

Figure 12. Response of the surge tank.

2.3. Response of Surge Tank Due to Variations of Tank Cross-Sections

In this research, the diameter of surge tank (D) varies $\pm 20\% D$ to investigate the response of the surge tank. Results showed that variations of the maximum values of head pressure fluctuation in the surge tank versus diameter values have a reverse trend in a way that the values decreased with an increase in D values. As illustrated in Figure 13, the maximum value of head pressure fluctuation increased from 9.10 m in D = 6 m to 9.54 m in D = 4.08 m. On the other hand, with an increase of D value from 6.0 m to 7.2 m, maximum values of head pressure fluctuation decreased from 9.10 m to 8.77 m.

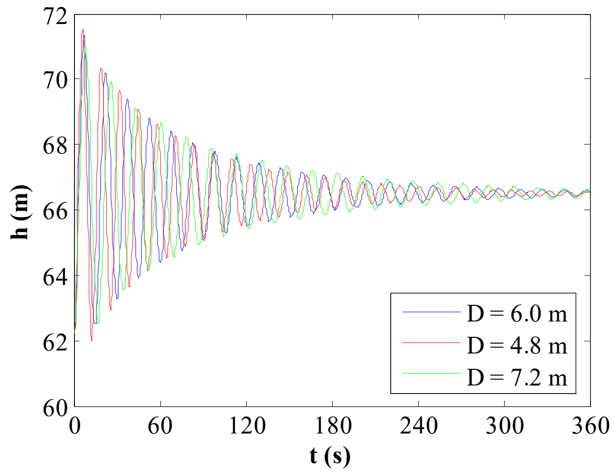

Figure 13. Variations of head pressure fluctuations for various values of surge tank diameter.

Furthermore, variations in flow velocity in the transient state versus different values of surge tank diameter were illustrated in Figure 14. Qualitatively, the results indicated that the maximum difference of flow velocity values in the node (just under the surge tank) rose from 13.76 m/s to 16.75 m/s when D values increased from 6.0 m to 7.2 m. In contrast, the maximum difference in flow velocity declined from 13.76 m/s in D = 6.0 m to 10.66 m/s in D = 4.08 m.

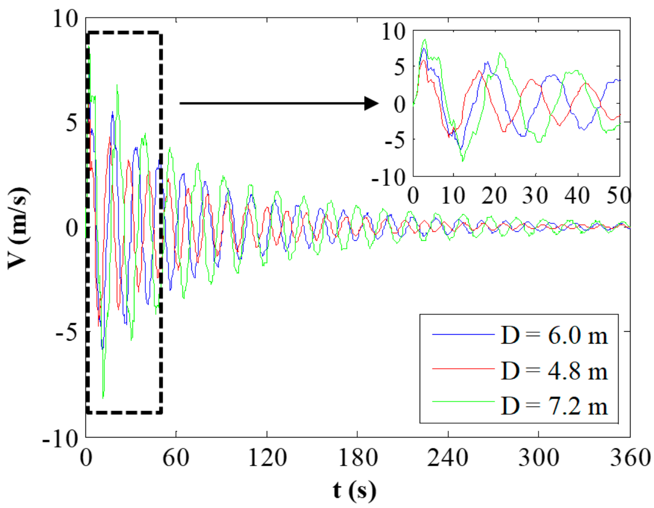

Figure 14. Variations of flow velocity fluctuations for various values of surge tank diameter.

2.4. Transient Flow Upstream of the Surge Tank

Due to the existing majority of pipe length between node 1 and node 5, Figure 15 demonstrated variations in head pressure and flow velocity between nodes 1 and 5 which are placed in the middle and last sections of the pipeline. The results demonstrated that the maximum value of the difference in the head pressure has a downward trend, decreasing from 8.62 m in node 5 to zero in node 1. In contrast, the maximum difference in the flow velocity increased from 16.25 m/s in node 5 to 18.52 m/s in node 1. The minimum and maximum head pressure values are presented in Figure 16. According to Figure 16, the maximum head pressure values were 6.62 m, 4.81 m, and 3.12 m for nodes 4, 3, and 2, respectively.

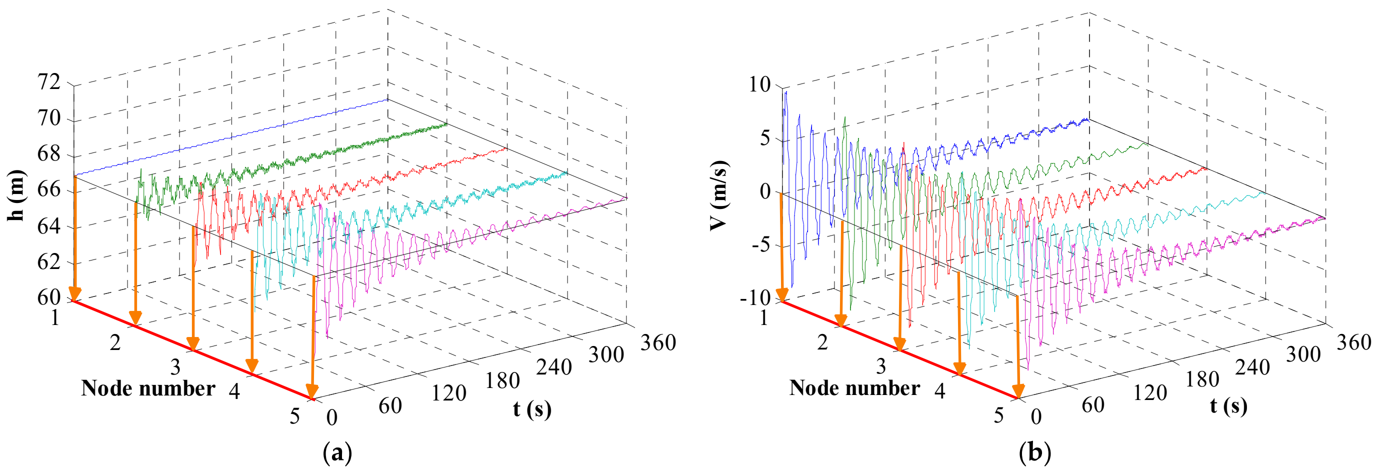

Figure 15. Variations upstream pipeline of surge tank for nodes 1 to 5: (**a**) head pressure and (**b**) flow velocity.

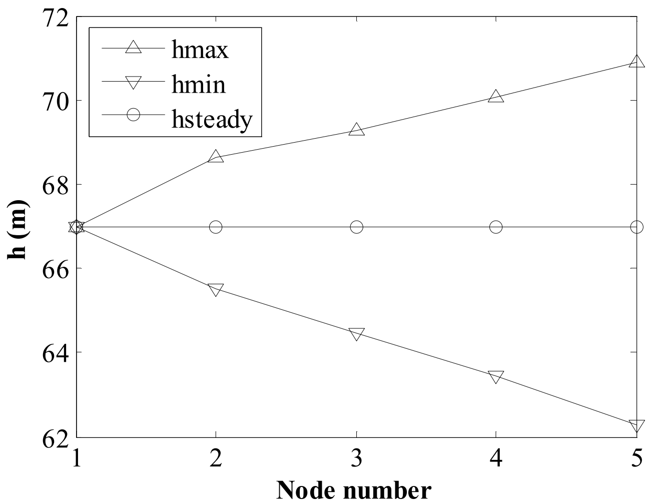

Figure 16. Minimum and minimum values of head pressure at nodes 1 to 5.

2.5. Effects of Surge Tank Inlet Diameter on Transient Flow Upstream of the Surge Tank

As mentioned in the previous section, the maximum difference in the head pressure was on the decline and additionally, this trend remained with variations in the surge tank inlet diameter. Figure 17a demonstrated that, for d = 2.72 m, the maximum difference in the head pressure declined from 8.73 m in node 5 to zero in node 1. Moreover, for d = 4.08 m, the maximum difference in the head pressure decreased from 9.01 m in node 5 to zero in node 1 (see Figure 17b). Therefore, it can be said that variations in the surge tank inlet diameter do not prevent the decrease in the fluctuation of head pressure upstream of the surge tank.

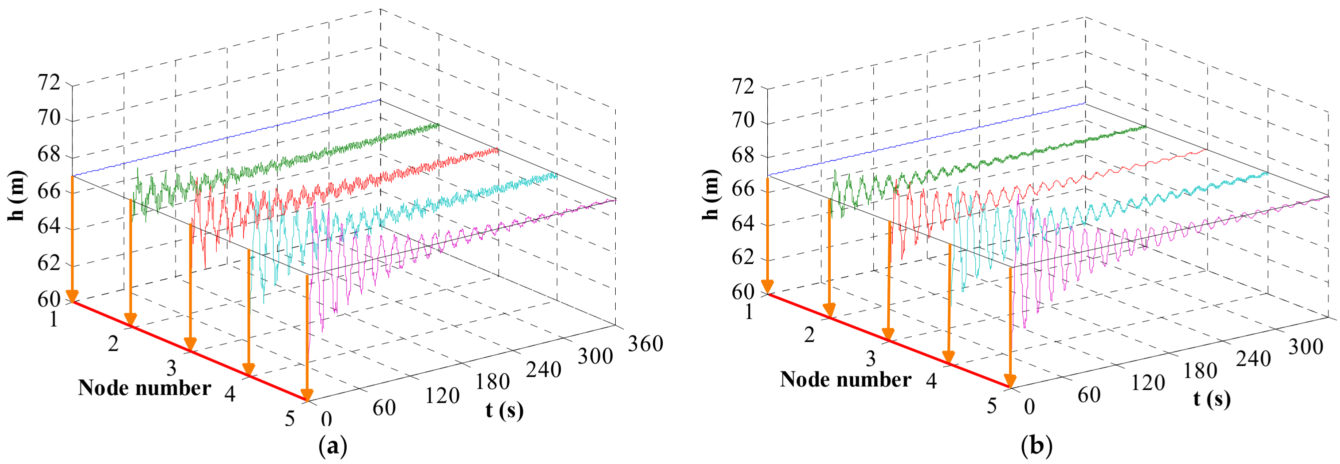

Figure 17. Variations of maximum difference in the head pressure for nodes 1 to 5 versus various values of surge tank inlet diameter: (**a**) d = 2.72 m and (**b**) d = 4.08 m.

Table 1 presents flow velocity values for nodes 1 to 5 in the various values of the surge tank inlet diameter. As seen in Table 1, the maximum difference in the flow velocity upstream of the surge tank has an upward trend when the inlet diameter of the surge tank increased from 2.72 m to 4.08 m. In fact, fluctuations of flow velocity upstream of the surge tank were affected by a decrease in inlet diameter (d).

Table 1. Flow velocity values for various values of surge tank inlet diameter at pipeline upstream.

Node Number	d (m)	v_{max} (m/s)	v_{min} (m/s)	$v_{max} - v_{min}$ (m/s)
1	2.72	8.69	−8.91	17.60
	3.40	9.64	−8.88	18.52
	4.08	10.26	−8.80	19.06
2	2.72	8.67	−8.16	16.83
	3.40	9.57	−8.75	18.32
	4.08	10.15	−8.61	18.76
3	2.72	8.50	−7.92	16.42
	3.40	9.39	−8.04	17.43
	4.08	9.88	−8.24	18.12
4	2.72	8.46	−7.65	16.11
	3.40	9.02	−7.78	16.80
	4.08	9.31	−8.33	17.64
5	2.72	8.34	−6.96	15.30
	3.40	8.78	−7.47	16.25
	4.08	8.99	−7.75	16.74

2.6. Effects of Surge Tank Diameter on the Transient Flow Upstream of the Surge Tank

Figure 18a,b depicted fluctuations of head pressure upstream of the surge tank for different values of D. As seen in Figure 18a,b, the maximum difference in pressure head values in the surge tank upstream decreased as the diameter of the surge tank increased. For D = 4.8 m, the maximum difference in the pressure head decreased from 9.17 m at node 5 to zero at node 1 (see Figure 18a) and similarly, for D = 7.2 m, the maximum value of the difference in the pressure head declines from 8.71 m at node 5 to zero at node 1 (see Figure 18b).

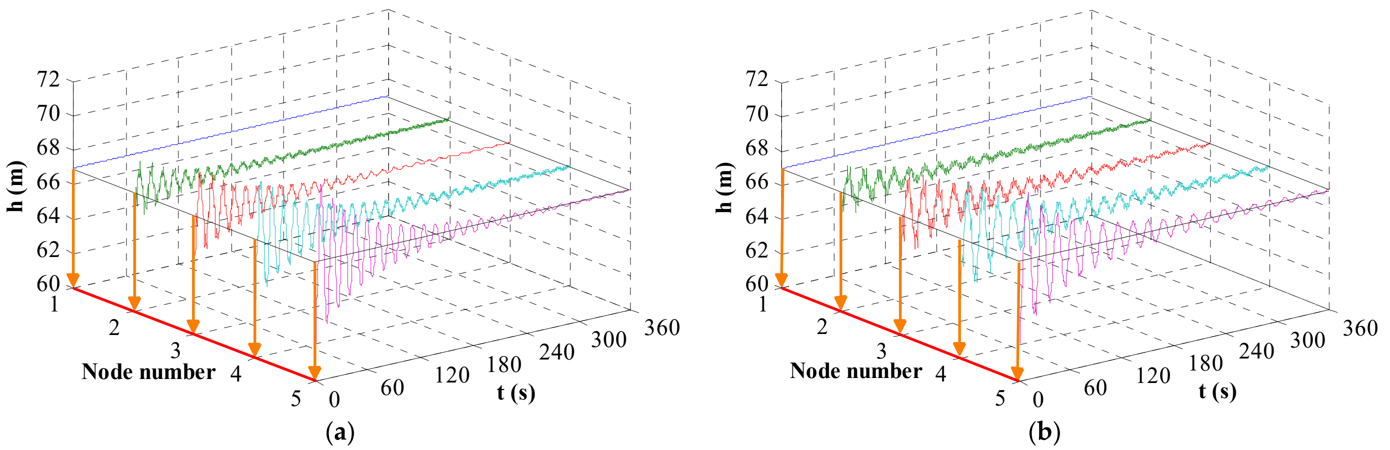

Figure 18. Fluctuations of head pressure upstream of surge tank with different diameters: (**a**) D = 4.8 m and (**b**) D = 7.2 m.

Figure 19a,b illustrate the fluctuation of flow velocity upstream of the surge tank for various values of the surge tank diameter. According to Figure 19a,b, the maximum difference in the flow velocity has an upward trend upstream of the surge tank as the diameter of the surge tank increases. For D = 4.8 m, the maximum difference in the flow velocity increased from 14.7 m/s in node 5 to 16.8 m/s in node 1 (see Figure 19a).

Additionally, the maximum difference in the flow velocity rose from 17.87 m/s in node 5 to 19.37 m/s in node 1 for *D* = 7.2 m (see Figure 19b).

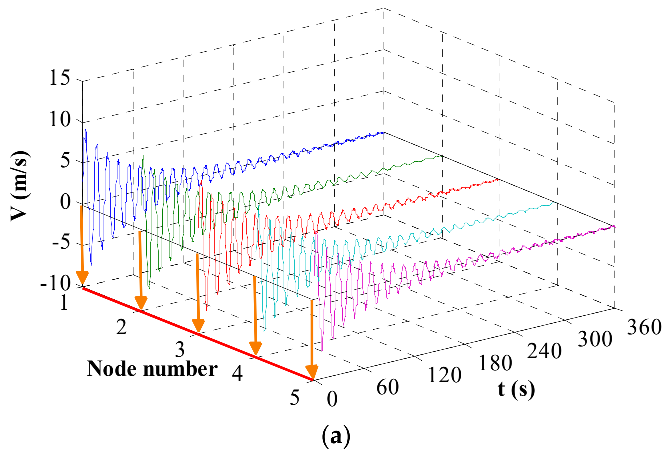

Figure 19. Maximum difference in the flow velocity at upstream of the surge tank with different diameters: (**a**) *D* = 4.8 m and (**b**) *D* = 7.2 m.

2.7. Simultaneous Effects of Surge Tank Characteristics on the Surge Tank Response

Table 2 presents the maximum difference in the pressure head for the three values of surge tank diameter (*D*) and three values of surge tank inlet diameter (*d*). In fact, nine combinations for *d* and *D* values were provided. As seen in Table 2, for the minimum value of surge tank diameter (*d* = 4.8 m), the fluctuation of head pressure in the surge tank stood at the maximum level when *d* values had an intermediate level (*d* = 3.4 m). Furthermore, values of head pressure fluctuation for both minimum and maximum values of surge tank inlet diameter are approximately the same. Overall, it can be inferred from Table 2 that for all the *D* values, the value of head pressure fluctuation in the surge tank stood at the minimum level for the maximum value of surge tank diameter. In the case of *D* = 6 m, the minimum value of head pressure fluctuation obtained was 8.95 m for *d* = 4.08 m, for instance.

Table 2. Maximum fluctuations in the pressure head for the surge tank response.

D (m)	***d*** **(m)**		
	2.72	3.40	4.08
4.8	9.27	9.54	9.30
6.0	9.10	9.10	8.95
7.2	8.88	8.77	8.66

In Table 3, the minimum and maximum values of flow velocity fluctuations at node 8 obtained 7.03 m/s and 24.67 m/s, respectively. In fact, the minimum level of fluctuation (7.03) was associated with *d* = 4.08 m and *D* = 4.8 m while the maximum values of fluctuation were due to *d* = 2.72 m and *D* = 7.2 m. According to the results, when the design of the surge tank with a low diameter and high inlet diameter is desirable, fluctuation of head pressure in the surge tank and fluctuation of flow velocity decreased along with the reduction of costs.

Table 3. Fluctuations in the transient flow velocity at the surge tank inlet (node 8).

D (m)	***d* (m)**		
	2.72	3.40	4.08
4.8	18.12	10.66	7.03
6.0	20.63	13.76	9.23
7.2	24.67	16.75	11.15

2.8. Simultaneous Effects of Surge Tank Characteristics on the Response of Upstream

Values of head pressure fluctuations upstream of the surge tank for each combination of *d* and *D* were given in Table 4. In the minimum value of surge tank diameter (*D* = 4.8 m) for nodes 2 and 5, head pressure fluctuation decreased with an increase in *d* values. On the contrary, this issue had a downward trend for nodes 3 and 4. Hence, it can be said that values of head pressure fluctuation in the middle section of the upstream pipeline did not stand at the minimum level with a lower diameter surge tank and higher value of surge tank inlet diameter. In nodes 3 to 5, head pressure fluctuations in the middle section of the diameter surge tank stood at a higher level for *d* = 2.72 m and 4.08 m than that of *d* = 3.4 m. While, for *D* = 6 m the head pressure fluctuations in node 2, decreased with an increase of *d* = 3.4 m.

Table 4. Head pressure fluctuations upstream of the surge tank for each combination of *d* and *D*.

Node Number	*D* (m)								
	4.8			6.0			7.2		
	d (m)			*d* (m)			*d* (m)		
	2.72	3.40	4.08	2.72	3.40	4.08	2.72	3.40	4.08
1	0	0	0	0	0	0	0	0	0
2	3.21	3.13	2.95	3.13	2.99	2.87	3.06	2.89	2.69
3	4.73	4.79	5.03	5.10	4.64	4.82	4.96	4.81	4.62
4	6.86	6.81	6.96	6.74	6.62	6.96	6.90	6.80	6.66
5	9.23	9.17	9.16	8.73	8.62	9.00	8.45	8.71	8.94

Generally, design purpose of the surge tank in the middle level of *d* and *D*, the head pressure fluctuations in the majority section of the upstream surge tank stood at the minimum level for both middle values of surge tank properties (*d* = 3.4 m and *D* = 6 m). Moreover, a high risk of water hammer occurrence is probable at the beginning of the upstream surge tank. Moreover, for *D* = 7.2 m, head pressure fluctuations decreased at nodes 2 and 4 with an increase of d values while, for node 5, this trend was increasing. Hence, it can be said that the design of a surge tank with high values of *D* and *d* causes to increase in the probability of water hammer occurrences.

Table 5 indicated flow velocity fluctuations in the surge tank upstream for each combination of *D* and *d* values. For the low value of *D*, fluctuation of flow velocity stood at the maximum level, as *d* was equal to 3.4 m. Moreover, for *D* = 6 m and 7.2 m, the inlet diameter values of the surge tank were 3.4 and 4.08 m and fluctuations of flow velocity were found to be maximum for *d* = 4.08 m. Furthermore, for each value of *d*, fluctuations of flow velocity at the surge tank upstream increased with an increase in the diameter of the surge tank.

Table 5. Fluctuations of transient flow velocity upstream of the surge tank for each combination of *d* and *D*.

Node Number	*D* (m)								
	4.8			6.0			7.2		
	d (m)			*d* (m)			*d* (m)		
	2.72	3.40	4.08	2.72	3.40	4.08	2.72	3.40	4.08
1	15.42	16.80	16.11	17.61	18.52	19.07	17.97	19.37	20.38
2	15.23	16.46	15.65	16.83	18.32	18.75	17.58	19.11	20.25
3	14.94	16.09	15.27	16.42	17.44	18.12	17.01	18.57	20.03
4	14.55	15.58	14.69	16.11	16.81	17.64	16.71	18.00	18.62
5	14.30	14.70	13.72	15.30	16.25	16.74	16.60	17.87	18.18

3. Conclusions

In this research, a numerical simulation of the water hammer phenomenon was conducted using MOC along with various boundary conditions. Responses of the surge tank and upstream pipeline of the surge tank to the variations of *d* and *D* variables were investigated. In this way, each of the *d* and *D* variables varied by $\pm 20\%$, and therefore, three levels of *d* (or *D*) were provided for each geometric factor. Thus, the following conclusions were drawn:

- Although the maximum fluctuation of head pressure in the surge tank for $d = 2.72$ m and 3.40 m remained constant values, head pressure for *d* of 2.72 m had lower fluctuations than that of $d = 3.40$ m.
- Results of MOC simulations indicated that variations of the maximum values of head pressure fluctuations in the surge tank decreased as the surge tank diameter became larger.
- At upstream of the surge tank (nodes 5 to 1), maximum values of head pressure and maximum values of transient flow velocity had downward and upward trends, respectively.
- The maximum values of fluctuation in the head pressure indicated a decreasing trend and then these variations were stable with variations of *d* values. Fluctuations of flow velocity in the pipeline of the surge tank upstream had a decreasing trend as *d* values decreased. Furthermore, the upward trend of head pressure fluctuations at the surge tank upstream remained constant with variations in surge tank diameter. For all diameters of the surge tank, minimum values of head pressure fluctuations took place for $d = 4.08$ m.
- Design of the surge tank with low *D* and high *d* causes the reduction of construction costs in a way that head pressure fluctuations in the surge tank and flow velocity in the pipeline decreased. In this state, fluctuations of head pressure in the middle sections of the pipeline upstream stood at the maximum level, and, additionally, negative consequences of the water hammer need to be prevented. Furthermore, the design of the surge tank with high values of *D* and *d*, the risk of water hammer at the vicinity of the surge tank is higher than other sections of the pipeline upstream.

The present study was a real-world problem in which ranges of *d* and *D* were generally limited. Although the effects of *d* and *D* values on the water hammer response of the surge tank were fully investigated by considering reasonable variations of *d* and *D*, the limitations of *d* and *D* values can be more focused. Moreover, one of the aims of this study was to reach minimizing the difference between values of $H_{\max}$ and $H_{\min}$ for the surge tank by the MOC. There is no denying the fact that the defined difference is in relation to the geometrical properties of water systems (i.e., values of *d* and *D*) and properties of pipelines such as the friction factor of the pipeline system. In this way, finding optimum values of *d* and *D* would play a key role in managing the water hammer that occurred in the power plant of power for Jiroft Hydroelectric Dam. Therefore, optimization techniques such as evolutionary algorithms (e.g., Genetic Algorithm [GA], Particle Swarm Optimization [PSO], Gravitational Search Algorithm [GSA], and Ant Colony Optimization [ACO]) can be employed in order to find the optimum values of d and D for minimizing the term of $H_{\max} - H_{\min}$ that was known as the first objective function. Furthermore, in order to obtain minimum costs of the power plant construction, a cost function can be defined as the second objective function. Another feasible improvement in the minimizing of $H_{\max} - H_{\min}$ is related to applying typical FDMs as implicit and explicit schemes in order to assess the accuracy level of solution to the governing equations of the water hammer.

Author Contributions: Conceptualization, M.M.-R. and M.N.; Methodology, M.M.-R. and M.N.; Software, M.M.-R. and M.N.; Validation, M.M.-R.; Formal Analysis, M.M.-R. and M.N.; Investigation, M.M.-R. and M.N.; Writing—Original Draft Preparation, M.M.-R. and M.N.; Writing—Review and Editing, M.M.-R. and M.N.; Visualization, M.M.-R. and M.N.; Supervision, M.M.-R. and M.N. All authors have read and agreed to the published version of the manuscript.

Funding: This research received no external funding.

Institutional Review Board Statement: Not applicable.

Informed Consent Statement: Not applicable.

Data Availability Statement: Not applicable.

Acknowledgments: Authors greatly appreciate reviewers' comments in order to improve the technical contents of the research work.

Conflicts of Interest: The authors declare no conflict of interest.

References

1. Wan, W.; Huang, W. Investigation on complete characteristics and hydraulic transient of centrifugal pump. *J. Mech. Sci. Technol.* **2011**, *25*, 2583–2590. [CrossRef]
2. Hur, J.; Kim, S.; Kim, H. Water hammer analysis that uses the impulse response method for a reservoir-pump pipeline system. *J. Mech. Sci. Technol.* **2017**, *31*, 4833–4840. [CrossRef]
3. Kim, S.G.; Lee, K.B.; Kim, K.Y. Water hammer in the pump-rising pipeline system with an air chamber. *J. Hydrodyn.* **2014**, *26*, 960–964. [CrossRef]
4. Rohani, M.; Afshar, M.H. Simulation of transient flow caused by pump failure: Point-Implicit Method of Characteristics. *Ann. Nucl. Energy* **2010**, *37*, 1742–1750. [CrossRef]
5. Guo, W.; Yang, J.; Teng, Y. Surge wave characteristics for hydropower station with upstream series double surge tanks in load rejection transient. *Renew. Energy* **2017**, *108*, 488–501. [CrossRef]
6. Liu, J.; Zhang, J.; Chen, S.; Yu, X. Investigation on maximum upsurge and air pressure of air cushion surge chamber in hydropower stations. *J. Press. Vessel. Technol.* **2017**, *139*, 031603. [CrossRef]
7. Riasi, A.; Tazraei, P. Numerical analysis of the hydraulic transient response in the presence of surge tanks and relief valves. *Renew. Energy* **2017**, *107*, 138–146. [CrossRef]
8. Duan, H.F.; Tung, Y.K.; Ghidaoui, M.S. Probabilistic analysis of transient design for water supply systems. *J. Water Resour. Plan. Manag.* **2010**, *136*, 678–687. [CrossRef]
9. Kim, S.H. Design of surge tank for water supply systems using the impulse response method with the GA algorithm. *J. Mech. Sci. Technol.* **2010**, *24*, 629–636. [CrossRef]
10. Collins, R.P.; Boxall, J.B.; Karney, B.W.; Brunone, B.; Meniconi, S. How severe can transients be after a sudden depressurization? *J. -Am. Water Work. Assoc.* **2012**, *104*, 243–251. [CrossRef]
11. Zhang, B.; Wan, W.; Shi, M. Experimental and numerical simulation of water hammer in gravitational pipe flow with continuous air entrainment. *Water* **2018**, *10*, 928. [CrossRef]
12. Bettaieb, N.; Taieb, E.H. Assessment of Failure Modes Caused by Water Hammer and Investigation of Convenient Control Measures. *J. Pipeline Syst. Eng. Pract.* **2020**, *11*, 04020006. [CrossRef]
13. Behbahani-Nejad, M.; Bagheri, A. The accuracy and efficiency of a MATLAB-Simulink library for transient flow simulation of gas pipelines and networks. *J. Pet. Sci. Eng.* **2010**, *70*, 256–265. [CrossRef]
14. Esmaeilzadeh, F.; Mowla, D.; Asemani, M. Mathematical modeling and simulation of pigging operation in gas and liquid pipelines. *J. Pet. Sci. Eng.* **2009**, *69*, 100–106. [CrossRef]
15. Wan, W.; Zhang, B. Investigation of water hammer protection in water supply pipeline systems using an intelligent self-controlled surge tank. *Energies* **2018**, *11*, 1450. [CrossRef]
16. Wan, W.; Zhang, B.; Chen, X.; Lian, J. Water hammer control analysis of an intelligent surge tank with spring self-adaptive auxiliary control system. *Energies* **2019**, *12*, 2527. [CrossRef]

17. Bazargan-Lari, M.R.; Kerachian, R.; Afshar, H.; Bashi-Azghadi, S.N. Developing an optimal valve closing rule curve for real-time pressure control in pipes. *J. Mech. Sci. Technol.* **2013**, *27*, 215–225. [CrossRef]
18. Zhou, J.; Xu, Y.; Zheng, Y.; Zhang, Y. Optimization of guide vane closing schemes of pumped storage hydro unit using an enhanced multi-objective gravitational search algorithm. *Energies* **2017**, *10*, 911. [CrossRef]
19. Wan, W.; Li, F. Sensitivity analysis of operational time differences for a pump–valve system on a water hammer response. *J. Press. Vessel. Technol.* **2016**, *138*, 011303. [CrossRef]
20. Karadžić, U.; Bulatović, V.; Bergant, A. Valve-induced water hammer and column separation in a pipeline apparatus. *Stroj. Vestn. J. Mech. Eng.* **2014**, *60*, 742–754. [CrossRef]
21. Hoeller, S.; Jaberg, H. A contribution to water hammer analysis in pumped-storage power plants. *Wasserwirtsch. Hydrol. Wasserbau Hydromechanik Gewässer Ökol. Boden* **2013**, *103*, 78–84.
22. Vasconcelos, J.G.; Klaver, P.R.; Lautenbach, D.J. Flow regime transition simulation incorporating entrapped air pocket effects. *Urban Water J.* **2015**, *12*, 488–501. [CrossRef]
23. Wang, C.; Yang, J.D. Water hammer simulation using explicit–implicit coupling methods. *J. Hydraul. Eng.* **2015**, *141*, 04014086. [CrossRef]
24. Dhakal, R.; Zhou, J.; Palikhe, S.; Bhattarai, K.P. Hydraulic Optimization of Double Chamber Surge Tank Using NSGA-II. *Water* **2020**, *12*, 455. [CrossRef]
25. Guo, Q.; Zhou, J.; Li, Y.; Guan, X.; Liu, D.; Zhang, J. Fluid-Structure Interaction Response of a Water Conveyance System with a Surge Chamber during Water Hammer. *Water* **2020**, *12*, 1025. [CrossRef]
26. Kubrak, M.; Malesińska, A.; Kodura, A.; Urbanowicz, K.; Bury, P.; Stosiak, M. Water Hammer Control Using Additional Branched HDPE Pipe. *Energies* **2021**, *14*, 8008. [CrossRef]
27. Zhang, K.; Zeng, W.; Simpson, A.R.; Zhang, S.; Wang, C. Water Hammer Simulation Method in Pressurized Pipeline with a Moving Isolation Device. *Water* **2021**, *13*, 1794. [CrossRef]
28. Chaudhry, M.H. Applied Hydraulic Transients, 3rd ed.Springer: New York, NY, USA, 2014.
29. Bergant, A.; Simpson, A.R.; Vìtkovsk, J. Developments in unsteady pipe flow friction modelling. *J. Hydraul. Res.* **2001**, *39*, 249–257. [CrossRef]
30. Pal, S.; Hanmaiahgari, P.R.; Karney, B.W. An Overview of the Numerical Approaches to Water Hammer Modelling: The Ongoing Quest for Practical and Accurate Numerical Approaches. *Water* **2021**, *13*, 1597. [CrossRef]